





Influence of curing conditions on the heat deflection temperature and Vicat softening temperature of LH285 MGS resin

Robert Szczepaniak¹, Przemysław Sapiński^{1*},
Naje Deefallah², Aneta Krzyżak³, Stanisław Oszczak⁴

¹ Faculty of Aviation, Polish Air Force University, ul. Dywizjonu 303 No. 35, 08-521 Dęblin, Poland

² Royal Saudi Air Force, Prince Sultan Air Base, 3H76+4P9, Industrial Area 16464, Al Kharj, Saudi Arabia

³ Mechanical and Electrical Engineering Faculty, Polish Naval Academy, ul. inż. Jana Smidowicza 69, 81-127 Gdynia, Poland

⁴ Institute of Navigation, Polish Air Force University, ul. Dywizjonu 303 No. 35, 08-521 Dęblin, Poland

* Corresponding author's email: p.sapinski@law.mil.pl

ABSTRACT

This paper presents the results of a study on the heat deflection temperature (HDT) and Vicat softening temperature (VST) of the LH285 MGS aerospace polymer resin, used as a matrix in ablative shielding composites. This topic is particularly relevant because, during ablative testing, the composite material undergoes partial combustion (ablative layer), while its remaining sections are exposed to elevated temperatures, leading to changes in viscoelastic properties that depend, among other factors, on VST and HDT. In this study, the authors examined aerospace resins cured under various conditions as recommended by the manufacturer. In addition to assessing changes in thermal properties due to material conditioning, the study also investigated the effects of heating rate and applied load magnitude, following the applicable standards for this type of material. The results indicate that resin heating influences HDT and VST values. Additionally, the indentation shape in the material varies with conditioning temperature. However, the choice of heating rate and load magnitude had a relatively minor impact on the results.

Keywords: epoxy resin, Vicat softening temperature, heat deflection temperature, surface profile examination.

INTRODUCTION

The advancement of every field in technical sciences is closely linked to the availability of construction materials. The stringent requirements for modern materials regarding their mechanical, physical, thermal, electrical, magnetic, and chemical properties limit the feasibility of using naturally occurring materials. Compared to raw natural materials, composites offer greater flexibility in tailoring the final product's characteristics to meet specific requirements by combining multiple components with distinct properties.

Epoxy resins are indispensable in today's industry. They serve as adhesives and matrix materials in advanced composites, where they are used for bonding or blending polymers. However, unmodified epoxies are inherently brittle, and their

low fracture energy raises concerns in certain applications. The adhesive properties of epoxy resins depend on curing conditions and temperature: they deteriorate at ambient temperatures but improve under high-temperature conditions.

One of the most common methods of modifying material properties is through the production of composites materials composed of at least two distinct phases. Due to their widespread applications across various industries, continuous improvements are being sought, particularly in terms of mechanical [1–5], ablative [6], and tribological properties [7, 8]. These enhancements are achieved either through innovative composite manufacturing techniques [9–11] or by incorporating modifiers into composite formulations.

Defining the performance requirements of materials necessitates an analysis of the operating

conditions of components made from them. Among the external factors influencing the reliability of machinery and equipment components, temperature plays a crucial role. In polymers, extreme temperature conditions can lead to changes in their state of aggregation. Therefore, testing newly developed materials for their thermal properties is essential. These properties are typically evaluated in laboratory conditions using heat deflection temperature (HDT) [12] and Vicat softening temperature (VST) [13] measurements.

Epoxy resins were first discovered in 1909 by Russian chemist Prileschajev, who observed that olefins react with peroxybenzoic acid to form epoxides—compounds later used in epoxy production alongside polyamines [14]. In 1936, two scientists Dr. Pierre Castan from Switzerland and Dr. S.O. Greenlee from the USA further developed the chemistry of epoxy resins that is widely applied today [15]. Currently, the specialty epoxy sector is a highly attractive industry, as it requires advanced expertise in formulation and technical support, making these skills highly valued [16]. The epoxy resins market size is estimated at 4.64 million tons in 2025, and is expected to reach 6.28 million tons by 2030, at a CAGR of 6.22% during the forecast period (2025–2030) (Figure 1) [17].

Epoxy resins contain two or more ring-like epoxy groups in the monomer. This group, also known as an epoxide or oxirane, may be located within the molecule's structure but is usually terminal. To achieve a cross-linked structure, the precursor resin must contain molecules with the functionality of two or more epoxy groups. The non-epoxy portion of the molecule can be aliphatic, cycloaliphatic, or highly aromatic. Alternatively, it may be non-hydrocarbon and potentially polar. It can also contain unsaturated bonds.

Many of today's industrial products would not exist without epoxies. Depending on their physical state, which can range from a low-viscosity liquid to a crystalline, high-melting-point solid—materials based on epoxy resins offer versatility in application. Their diverse chemical properties make them suitable for a wide range of industrial and everyday uses, as illustrated in Figure 2. There are seven key sectors that utilize epoxy resin-based products, which are particularly significant from both a strategic and economic perspective [17].

BACKGROUND AND MOTIVATION

Current aviation structures primarily use metals such as copper and aluminium. However, these materials present several challenges, including high weight, susceptibility to corrosion, and significant maintenance costs. The percentage of total structural weight attributed to composites in selected aircraft is illustrated in Figure 3. To address these issues, it is essential to explore alternative solutions beyond the current technologies. As a result, new composite materials have been developed to mitigate problems related to lightning strikes and ice accumulation.

The excellent strength-to-weight ratio of composites is also utilized in helicopters to maximize payload capacity and overall performance. In the past, Boeing Vertol used composites for rotorcraft fairings in the 1950s and developed the first composite rotor blades in the 1970s. Today, composite materials make up nearly 50% of the Boeing 787, resulting in an average weight reduction of 20% (Figure 4). Similarly, composites account for approximately 25% of the Airbus A380's structure.



Figure 1. Epoxy resin market CAGR (%), growth rate by region – 2015 [17]

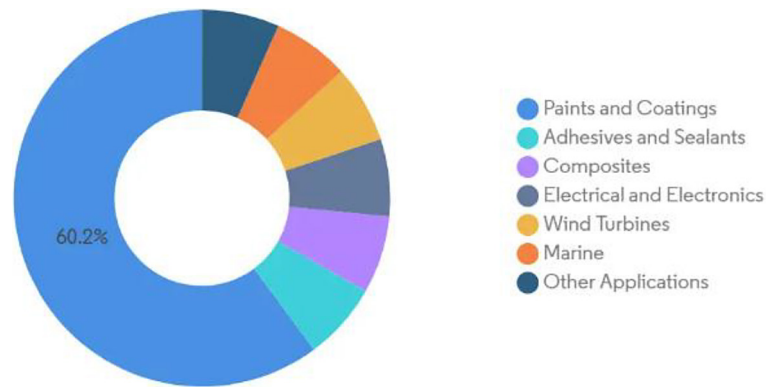


Figure 2. Epoxy resin market share by applications – 2024 [17]

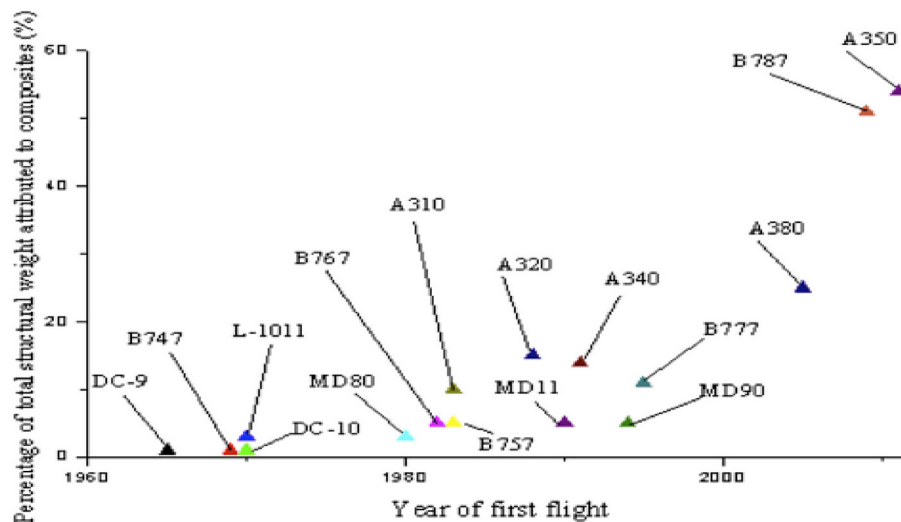


Figure 3. The percentage of the total structural weight attributed to composites [18]

Composites are now used in critical structural components of many modern helicopters. The F-35, a fifth-generation combat aircraft (Figure 5) designed to replace a wide range of aging fighter and strike aircraft, consists of 35% composite materials. Its design enhances stealth capabilities through features such as a trapezoidal mid-wing configuration, twin tail fins, and an internal weapons bay.

Composite materials must be properly designed to ensure they perform the intended functions [21]. Industrial materials companies are continuously developing new composite-based solutions for use in aircraft. For example, Hexcel has introduced HexWeb® Acousti-Cap®, a permeable cap material embedded into a honeycomb core, which helps reduce noise during takeoff and landing in Boeing 737 MAX engines. Additionally, Diab Group supplies Divinycell F, a thermoplastic foam used in seats and interior components of aircraft such as the Airbus A350 XWB [22].

Another sector of the aviation industry where resin-based composites are widely used is aviation propulsion. In the GE90 engine series (Figure 6), general electric (GE) has made significant investments in carbon fiber-reinforced epoxy resin composites to develop high-toughness fan blades. These composites were designed as an alternative to traditional titanium alloys. Compared to conventional titanium alloy fan blades, composite fan blades offer several advantages, including improved vibration resistance, lower noise levels, enhanced bird-strike resistance, and other performance benefits. The results demonstrate that high-toughness epoxy composites provide excellent safety and reliability in Boeing 777 engines while maintaining a high level of serviceability [23].

Moreover, composite structural elements have demonstrated high specific energy absorption (SEA) under crash loads through appropriate design and the initiation of suitable failure modes. The challenge lies in designing a crashworthy

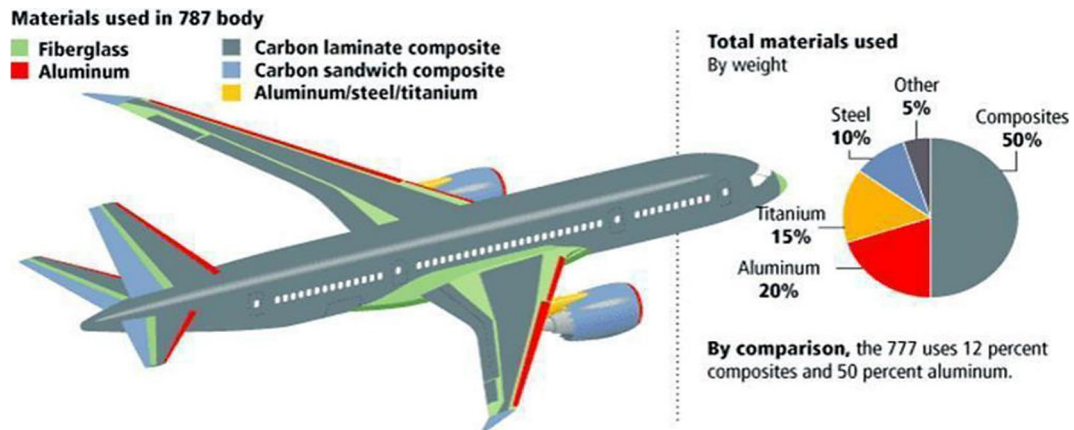


Figure 4. Composite materials in aerospace application [19]

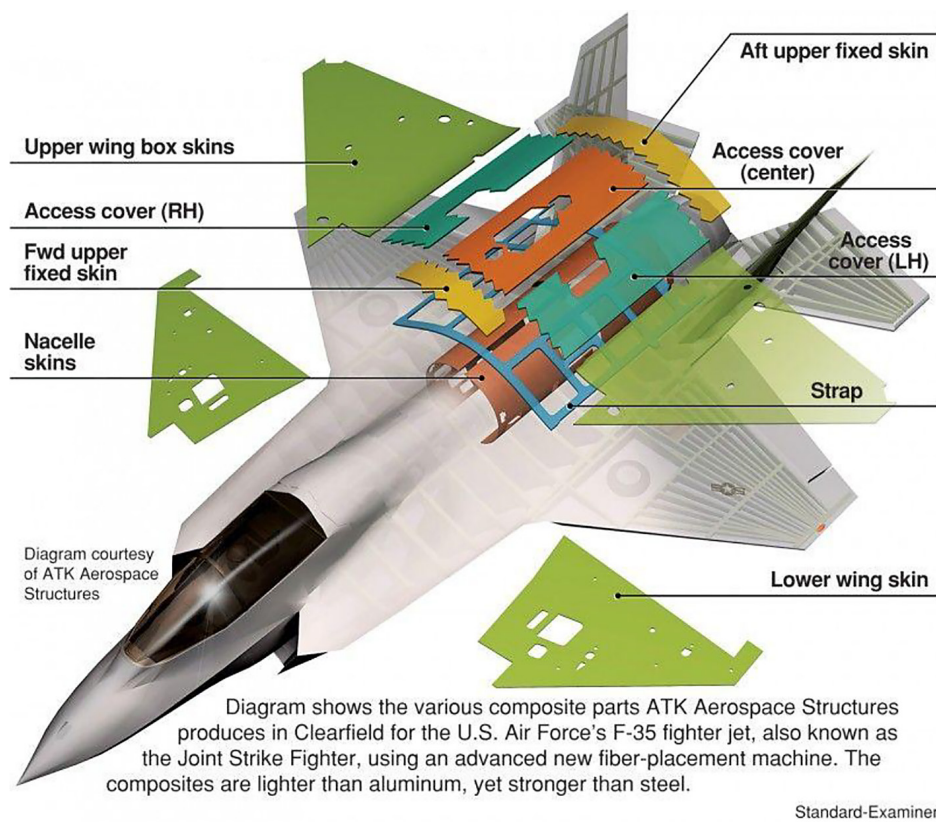


Figure 5. F-35 JSF composite parts [20]

aircraft structure such as a composite subfloor that serves a dual function: withstanding flight structural loads while also providing crash energy absorption under emergency conditions. For new composite aircraft, such as the Boeing 787, this requirement is outlined in Special Condition SC 25-07-05-SC, which mandates that the composite fuselage must exhibit a safety level equivalent to that of existing metallic aircraft [25].

Aircraft are exposed to several significant environmental hazards that can lead to serious

accidents or reduced performance, making aviation inherently risky. One of the major concerns is lightning strikes, which can impact various aircraft components, such as the fuselage. When a strike occurs, it generates a high electrical current that, if not properly dissipated, can penetrate the aircraft and cause hazardous fires. These direct effects may also result in the vaporization of resin in the immediate strike area, potentially leading to burn-through of the composite laminate [26].



Figure 6. GE9X engine cross section visualization [24]

Currently, research is being carried out to determine the softening temperature of polymer-based materials with additives, which are often subjected to temperature influences [27]. This results in the need to conduct research on resin-based materials used in aviation technology.

The novelty of this study lies in its targeted investigation of the thermal softening behavior (VST and HDT) of LH285 MGS epoxy resin, a material primarily used in aerospace ablative shielding applications. While LH285 is known for its high-performance characteristics, there is a lack of publicly available data on its viscoelastic response under post-ablation thermal exposure conditions, which is critical for ensuring the integrity of the non-ablated structural zones of the composite.

Unlike previous studies that typically focus on the ablation layer itself or on the high-temperature resistance of composites as a whole, this research isolates the thermo-mechanical transitions of the polymer matrix in response to standardized thermal loads. By varying curing conditions, heating rates, and load magnitudes, the study explores the influence of process history on softening behavior, providing engineers with valuable insight into design margins and safety thresholds for such materials under sub-critical thermal stress.

Furthermore, the research introduces profilometric mapping of indentation topography after VST testing, highlighting morphological changes that are not commonly evaluated in standard thermal testing of epoxy systems. This aspect may contribute to refining material selection or predictive modeling in aerospace thermal protection systems.

EXPERIMENTS

The purpose of this study is to prepare and conduct an analysis of the thermal properties specifically, HDT under load and VST as well as the indirect optical properties of epoxy resin samples. The optical properties will be evaluated by measuring the samples using an optical profilometer after the Vicat test. After determining the characteristic temperatures of the manufactured materials, the affected surfaces will be mapped using an optical profilometer to analyze the impact of the Vicat test pin.

Scope of the study:

- Production of epoxy resin samples using the free molding method.
- Conditioning of two groups of samples in a climatic chamber for 24 hours at 55 °C and 80 °C.
- Conducting experimental tests on epoxy resin samples, including the determination of:
 - Vicat softening temperature (VST),
 - heat deflection temperature (HDT),
 - optical observations of the samples after the VST test.

Research methods

The experimental methods for determining the softening point using the Vicat method and the deflection temperature under load for plastics are standardized by the European Committee for Standardization. These methods are defined in International Standard ISO 306 for VST and International Standard ISO 75-2 for HDT. These standards precisely describe the shape and dimensions of the test specimens.

According to the standard, the samples for VST tests must be square (i.e., length = width) and within the following dimensional ranges [28]:

- Length (L) = Width (B) ≥ 10 mm,
- Thickness (H): $3 \text{ mm} \leq H \leq 6.5 \text{ mm}$.

For the deflection temperature under load (HDT) test, the required specimen shape is a rectangular beam with a rectangular cross-section, where length > width > thickness. The standard recommends the following dimensions [29]:

- Length (L): 80 ± 2.0 mm,
- Width (B): 10 ± 0.2 mm,
- Thickness (H): 4 ± 0.2 mm.

The test specimens were produced using the free casting method in silicone molds. This method ensures high shape repeatability, which

is crucial given the small dimensional tolerance required for HDT tests. Additionally, it allows for the simultaneous casting of multiple specimens in a single, small mold.

For this research, the Instron HV6X instrument was used to test the samples (Figure 7a and 7b). The HV6X is one of the most versatile and technically advanced instruments for determining HDT and VST in various thermoplastic and composite materials, complying with the following International Standards:

- ASTM D648 and ASTM D1525,
- ISO 75-1/-2/-3 and ISO 306.

The HV6X is equipped with independent working stations that measure the temperature at which the specimen undergoes a predefined deflection or penetration under a specific load while being heated. This process occurs at a defined heating rate in a silicone oil bath, with temperatures reaching up to 300 °C. The instrument is electronically controlled by a microprocessor via a touchscreen interface. Additionally, it uses LVDT transducers and independent thermos resistances at each station to ensure high accuracy and repeatable results. At the end of the test, the cooling cycle starts automatically.

After determining the Vicat softening point, the surface roughness of the samples was analyzed using a non-contact optical profilometer. Profilometry is a technique used to extract topographical data from the surface, which can be captured as a single point, a line scan, or a full three-dimensional scan. The primary objective of profilometry is to obtain information about surface morphology, step heights, and surface roughness.

The principle of operation of this device is based on scanning the examined object with a beam of visible white laser light. When the light reaches the surface of the sample, it is reflected, refracted, and scattered, causing interference in the returning light wave, which is then recorded by the device's detector. This process enables the acquisition of precise data on the geometry of the tested surface. Additionally, specialized software allows for the generation of a 3D surface model.

The surface roughness measurements were conducted using the MicroProf 100 (Figure 8a and 8b), a device manufactured by the German company FRT. This system enables extremely accurate, non-contact surface measurements in compliance with international standards. The device is designed to analyze samples with maximum dimensions of 150 × 100 × 50 mm and a maximum weight of 5 kg. It is equipped with a movable, motor-controlled table for sample placement. The system operates using

Determination of the Vicat softening temperature

The test methodology for determining the VST is specified in the International Standard ISO 306. These standard outlines four methods for determining the VST of thermoplastic materials [28]:

- Method A50: using a force of 10 N and a heating rate of 50 °C/h,
- Method B50: using a force of 50 N and a heating rate of 50 °C/h,
- Method A120: using a force of 10 N and a heating rate of 120 °C/h,
- Method B120: using a force of 50 N and a heating rate of 120 °C/h.

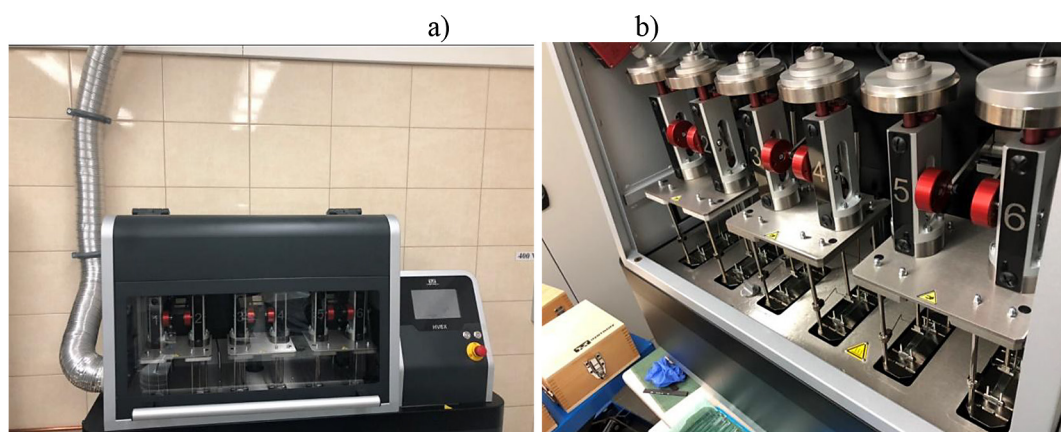


Figure 7. The HV6X instrument: a) general view, b) view of the measuring stations



Figure 8. MicroProf 100 device: a) general view, b) specimen mouting method

These methods are applicable only to thermoplastics and provide a measure of the temperature at which thermoplastics begin to soften rapidly. The test consists of determining the temperature at which a flat indenter reaches a depth of 1 mm below the surface of the test sample. The sample is placed horizontally, and the end of the indenter presses the sample with a defined perpendicular force. The process occurs under increasing temperature conditions. The temperature, measured as close as possible to the point where the indenter reaches 1 mm, expressed in degrees Celsius, is known as the VST.

Measuring apparatus and measurement station

The main components of the measuring apparatus and measurement station are [24]:

- Heating equipment – the heating equipment must have temperature control to allow the temperature to increase uniformly at a rate of $(50 \pm 5)^{\circ}\text{C/h}$ or $(120 \pm 10)^{\circ}\text{C/h}$. The heating equipment typically consists of a liquid-filled heating bath, in which the test specimen is immersed to a depth of at least 35 mm. Suitable heat transfer media include liquid paraffin, transformer oil, glycerol, and silicone oil, though other liquids can be used.
- Test frame assemblies – the test frame consists of a rod and frame equipped with a support plate or another suitable load-application device, all held in a rigid metal frame.
- Indenting tip – the tip is flat and perpendicular to the axis of the rod, and its surface must be

free from burrs. Weights are applied centrally to the rod, ensuring that the total load applied to the test specimen is (10 ± 0.2) N for methods A50 and A120, and (50 ± 1) N for methods B50 and B120.

- Penetration-measuring device – this instrument measures the penetration of the indenting tip into the test specimen with an accuracy of ± 0.01 mm.
- Temperature-measuring device – this device measures temperature within a range accurate to ± 0.5 $^{\circ}\text{C}$.

Determination of the temperature of deflection under load

The methodology for determining HDT is specified in the International Standard ISO 75, which consists of three parts. Part ISO 75-2 specifies methods for applying different values of constant bending stress, meaning the nominal value of the stress applied to the outer surface of the specimen at half the distance between the supports. The ISO 75-2 standard is dedicated to plastics and ebonite and contains three methods [25]:

- Method A – a bending stress of 1.80 MPa,
- Method B – a bending stress of 0.45 MPa,
- Method C – a bending stress of 8.00 MPa.

The three-point loading method is used in ISO 75-2. In this test, the area of uniform stress is small and concentrated under the center loading point. The temperature is raised at a constant rate of $(120 \pm 10)^{\circ}\text{C/h}$, and measurements are made to

record the temperature value when the standard deflection associated with an increase in bending strain is reached. The standard deflection is a function of the height h , the span used, and the flexural strain increase as given in ISO 75-2 or ISO 75-3. It is calculated using Formula 1:

$$\Delta s = \frac{L^2 \cdot \Delta \varepsilon_f}{600 \cdot h} \quad (1)$$

where: Δs is the standard deflection, in millimeters; L is the span, in millimeters, between the lines of contact of the test specimen and the specimen supports; $\Delta \varepsilon_f$ is the flexural-strain increase, in per cent; h is the thickness, in millimeters, of the test specimen.

The standard deflection values for different test-specimen heights for 80 mm length \times 10 mm width specimens are shown in Table 5. Moreover, in the three-point loading method, the force applied to the test specimen is given, in newtons, as a function of the flexural stress:

$$F = \frac{2\sigma_f \cdot b \cdot h^2}{3L} \quad (2)$$

where: F is the load, in newtons; σ_f is the flexural stress, in megapascals, at the test-specimen surface; b is the width, in millimetres, of the test specimen; h is the thickness, in millimetres, of the test specimen; L is the span, in millimetres, between the supports.

Measuring apparatus and measurement station

The main parts of the measuring apparatus and the measurement station are:

- Generation of bending stress apparatus – this consists of a rigid metal frame in which a rod can move freely in the vertical direction. The rod is fitted with a weight-carrying plate and a loading edge. The base of the frame is equipped with test-specimen supports, and both the supports and the vertical members of the frame are made of a material with the same coefficient of linear expansion as the rod (Figure 18).
- Heating equipment – this includes a heating bath containing a suitable liquid, a fluidized bed, or an air oven. For heat transfer media other than gas (air), the test specimen shall be

immersed to a depth of at least 50 mm. The heating equipment should have a control unit to ensure the temperature is raised at a uniform rate of $(120 \pm 10)^\circ\text{C/h}$.

- Weights – a set of weights is provided so that the test specimen can be loaded to the required flexural stress.
- Temperature-measuring instrument – this may be any suitably calibrated temperature-measuring device with an appropriate range, accurate to 0.5°C or less.
- Deflection-measuring instrument – this may be a calibrated micrometer dial gauge or any other suitable instrument capable of measuring the deflection at the midpoint between the test-specimen supports to within 0.01 mm.
- Micrometers and gauges – these are used to measure the width and thickness of the test specimens. They must be accurate to 0.01 mm.

Epoxy used for the preparation of the specimens

Epoxy resin L285 is produced by the German company Hexon. It is a laminating product with an aviation certificate issued by the German Federal Aviation Authority. This resin is intended for the production of composites reinforced with aramid, glass, and carbon fibers. The hardener used to initiate the cross-linking process of this resin is a substance designated as H285, which is added according to the recommended weight ratio of 100:40. There are two different hardeners dedicated to this epoxy: H286 and H287. They have the same mixing ratio and can be combined in any proportion. The conditioning process at a temperature of $50\text{--}55^\circ\text{C}$ ensures that the resin meets the standards defined for materials intended for the production of gliders and motor gliders, which include operating temperature limits in the range from -60 to 54°C . Heating at 80°C ensures compliance with similar criteria for motor airplanes, where the operating temperatures range from -60 to 72°C . The use of L285 resin and hardener H285 without heating is possible, but the manufacturer does not recommend this process. Depending on the hardener used, the working time ranges from 45 minutes to 5 hours [30] (Table 1, 2).

The epoxy resin and hardener are stored in pre-packed, separate containers. First, the two components were mixed in the proportion

Table 1. Specification of L285 epoxy resin and H285 hardener [30]

Parameter	Laminating resin L285	Hardener H285
Density [g/cm ³]	1.18–1.23	0.94–0.97
Viscosity [mPa·s]	600–900	50–100
Epoxy equivalent [g/equivalent]	155–170	-
Epoxy value [equivalent/100 g]	0.59–0.65	-
Refractory index	1.525–1.5300	1.5020–1.5500

Note: Measuring conditions: measured at 25 °C

Table 2. Mechanical data of LH285MGS epoxy resin [30]

Mechanical data of neat resin	
Density [g/cm ³]	1.18–1.20
Flexural strength [N/mm ²]	110–120
Modulus of elasticity [kN/mm ²]	3.0–3.3
Tensile strength [N/mm ²]	70–80
Compressive strength [N/mm ²]	120–140
Elongation of break [%]	5.0–6.5
Impact strength [kJ/m ²]	45–55
Water absorption 24 h [%] at 23 °C 7 d [%]	0.20–0.30 0.60–0.80
Curing: 24 h at 23 °C (74 °F) + 15 h at 60 °C (140 °F)	
Typical data according to WL 5.3203 pp. 1–2 of the German aviation materials manual	

recommended by the manufacturer. The PS2100 R2 laboratory scales by Radwag, with a measurement accuracy of ± 0.01 g, were used to measure the mass of the epoxy resin and hardener. The ingredients were then gently mixed to avoid incorporating air into the solution. The next step was to place the vessel with the mixture in an ultrasonic cleaner for about 5 minutes to accelerate the removal of air bubbles. After the vessel was removed from the apparatus, the contents were mixed again to achieve the required homogenization of the liquid. The moldings were then carefully cast into both types of specimens to obtain the desired thickness. The specimens were placed on the horizontal surface of the laboratory table. The entire process of casting and cross-linking of the resin took place at room temperature RT, around 23–24 °C.

After 24 hours, the samples were removed from the silicone molds and divided into three groups of twenty-four pieces. Two groups were subjected to heating at 55 °C or 80 °C for 15 hours, while the remaining samples were not subjected to this process (Figure 15a and 15b). The samples were heated in the WKL 64 climatic chamber, manufactured by the German company Weiss. Thanks to the electronic control of the

heating process, the machine maintained the desired temperature with an accuracy of ± 0.1 °C.

The prepared specimens are summarized in Tables 3. The nomenclature of the specimens is related to the conditioning temperature and the application of the test method type. This division and nomenclature will be used throughout the remainder of the engineering study. The tables also include the dimensions of the samples, which were measured using an electronic caliper and a micrometer, ensuring a measurement accuracy of ± 0.01 mm. Each sample was inspected, and any imperfections, such as burrs, were removed with low-grit sandpaper.

RESULTS

Vicat softening temperature

The VST test began with the configuration of the Instron Bluehill HV program installed on a notebook computer. All test parameters were configured, including test type (VST), standard (ISO 306), load variant, temperature rise rate (both load and oil heating rates), initial temperature (23 °C), and conditioning time (the duration

Table 3. Specimens for VST and HDT test numbers and parameters

Method parameters	Specimen number (heating at 23–24 °C)	Specimen number (heating at 55 °C)	Specimen number (heating at 80 °C)
VST: A50 HDT: A	RT01	5501	8001
	RT02	5502	8002
	RT03	5503	8003
	RT04	5504	8004
	RT05	5505	8005
	RT06	5506	8006
VST: B50 HDT: B	RT07	5507	8007
	RT08	5508	8008
	RT09	5509	8009
	RT10	5510	8010
	RT11	5511	8011
	RT12	5512	8012
VST: A120 HDT: C	RT13	5513	8013
	RT14	5514	8014
	RT15	5515	8015
	RT16	5516	8016
	RT17	5517	8017
	RT18	5518	8018
VST: B120 HDT: none	RT19	5519	8019
	RT20	5520	8020
	RT21	5521	8021
	RT22	5522	8022
	RT23	5523	8023
	RT24	5524	8024

for which the sample is immersed in the oil before starting the test, set to 5 minutes). This conditioning time is crucial for ensuring reliable results, as it allows the temperature of both the sample and the oil to equilibrate before starting the test. Next, the samples were placed in the measuring stations, maintaining their recommended position and ensuring that a minimum distance of 3 mm between the indenter tip and the sample edge was maintained. The following step involved entering the data into the program, such as the average thickness values of each tested sample. In the VST study, the total mass acting on the indenter at each station was kept the same. When calculating this, the empty weight of the bar was taken into account, enabling the operator to determine the weights to be placed on the stand. Afterward, the front panel of the device was closed, and the automatic temperature control for the heating bath was activated, stabilizing the temperature at 23°C. A program was then launched to automatically check the

heating and cooling systems of the station. It stabilized the temperature, loaded the samples, and immersed them in the heating liquid. Once this was completed, the proper part of the study began, which involved the displacement of the indenter tip and the recording of temperatures rising at a steady pace. The test was concluded either when a 1 mm depression was achieved in the last sample or when the test was manually interrupted. Cooling then started automatically, reducing the temperature of the liquid to the initial value. The procedure described above was repeated for each subsequent measurement. The results of the VST tests are presented in the form of a diagram showing the relationship between cavity depth and temperature. Each line represents measurements from different stations, and thus different samples. The graph in Figure 9 shows an example of tests results for several individual samples. Table 4 provides a summary of all test results.

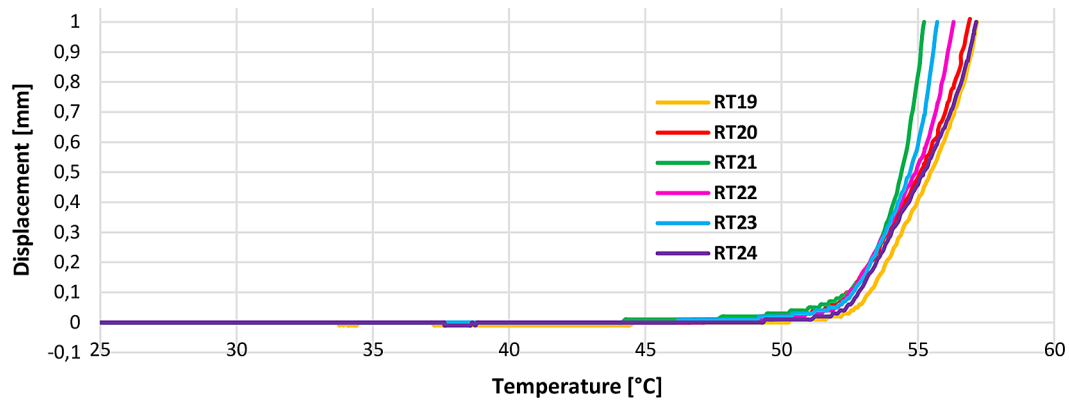


Figure 9. VST B120/RT graph of the dependence of deflection as a function of temperature

Table 4. Results of VST temperature measurements under different conditions

Load [N]	Heating rate. [°C/h]	Preparation temperature [°C]	VST temp. average [°C]	VST temp. median [°C]	VST temp. min. [°C]	VST temp. max. [°C]	Standard deviation [°C]
10	50	23	55.53	55.50	54.00	57.10	1.505
10	120	23	59.23	59.45	58.30	59.60	0.488
50	50	23	53.03	52.95	52.90	53.30	0.175
50	120	23	56.40	56.60	55.20	57.20	0.815
10	50	55	73.97	73.95	73.80	74.20	0.137
10	120	55	76.93	76.95	76.20	77.70	0.493
50	50	55	71.65	71.85	70.50	72.40	0.666
50	120	55	74.78	74.90	73.30	75.70	0.808
10	50	80	84.30	84.25	83.90	84.90	0.341
10	120	80	87.43	87.70	85.60	88.10	0.927
50	50	80	82.93	82.90	82.70	83.20	0.186
50	120	80	85.93	86.00	85.70	86.10	0.186

Heat deflection temperature

The HDT test began with connecting the Instron HV6X test stand to a computer via an Ethernet cable. Using Instron's Bluehill HV software installed on the computer, all the parameters for the test were configured, including the test type (HDT), ISO standard (ISO 75-2), option (A, B, or C), the rate of temperature increase (120 °C/h), the starting temperature (23 °C), and the pre-conditioning time. This pre-conditioning time is crucial for the reliability of the results, as it allows the temperature of the fitting and the oil to stabilize before starting the test.

Next, the samples were placed in the measurement stations, ensuring they were positioned correctly in the recommended middle position. The mean physical dimensions of each sample were then entered into the Bluehill program. Based on these dimensions, the software calculated the

load required to achieve the necessary bending stress value. These calculations took into account the weight of the bar, allowing the operator to determine which additional weights needed to be added to the stand. Additionally, the program's dimensions were used to determine the individual deflection standard for each fitting.

The front panel of the device was then closed, and the automatic temperature control of the heating bath was activated. The test was initiated from the computer. Once the program started, the heating and cooling systems were checked, the temperature was stabilized, the samples were loaded, and they were immersed in the heating liquid.

The test proper began once the samples were fully immersed, during which each station recorded the occurring sample deformations and the temperature increase at a constant rate. The test concluded when the last fitting reached the standard deflection. Following this, the cooling

phase began, reducing the temperature of the liquid back to its initial value. The test results, along with the data points, were available in Excel format and in the Bluehill program's report. This procedure was repeated for each subsequent measurement. The results of the HDT tests were presented in the Figure 10 as a graph of the deflection values as a function of temperature. Each line represented a different measuring station, thus corresponding to the various samples. The all results are summarized in Table 5.

Examination of the specimen surface

One sample from each series, corresponding to the conditioning temperatures (room temperature, 55 °C, and 80 °C), was selected for testing. All three samples were tested using the VST method type B120, with a force of 50 N and a heating rate of 120 °C/h. The first step was to place the test object on the movable table of the device and secure it. This ensured that the movement of the sample table did not affect its position.

Next, in the computer program FRT MARK III controlling the profilometer, the measurement

range and the accuracy of the reading points were set. During the measurement, the fitting attached to the table moved under the laser beam, which scanned its surface line by line. Once all the measurement points were captured, a surface map of the fitting was displayed on the monitor. Based on this data, a 3D model of the sample was generated, and the topography near the cavity formed during the Vicat tests was analyzed (Figures 11–13).

The topography of the three types of samples along the red measurement line appears as a discontinuous line. This indicates that the profilometer did not register all points of the cavity geometry. The bottom surface of the hole was recreated only for the sample annealed at 80 °C. For the sample heated at 80 °C, individual measuring points were selected, while for the sample heated at room temperature, no measuring points were recorded.

Visualizing the top of the cavity in color shows that the interaction of the standardized measuring tip distorts the immediate vicinity of the cavity, creating a geometry resembling an expanding funnel. The clear resin, which lacked color, made it difficult for the profilometer to register

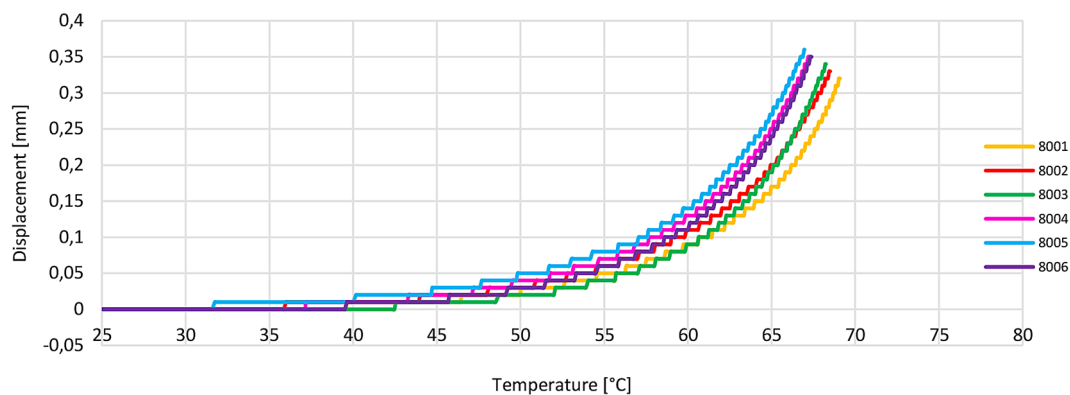


Figure 10. HDT graph of the dependence of deflection as a function of temperature 80 °C / A120

Table 5. Results of HDT temperature measurements under different conditions

HDT bending stress [MPa]	Preparation temperature [°C]	HDT temp. average [°C]	HDT temp. median [°C]	HDT temp. min. [°C]	HDT temp. max. [°C]	Standard deviation [°C]
0.45	23	53.25	53.35	52.80	53.60	0.339
1.8	23	51.12	51.10	50.90	51.50	0.223
8	23	47.85	47.85	47.40	48.20	0.321
0.45	55	67.92	68.05	67.20	68.40	0.515
1.8	55	63.05	63.20	60.20	65.40	1.693
8	55	52.50	54.50	43.40	55.20	4.594
0.45	80	75.15	75.30	74.10	75.80	0.616
1.8	80	67.92	67.85	67.00	69.00	0.794
8	80	57.98	58.10	57.60	58.20	0.264

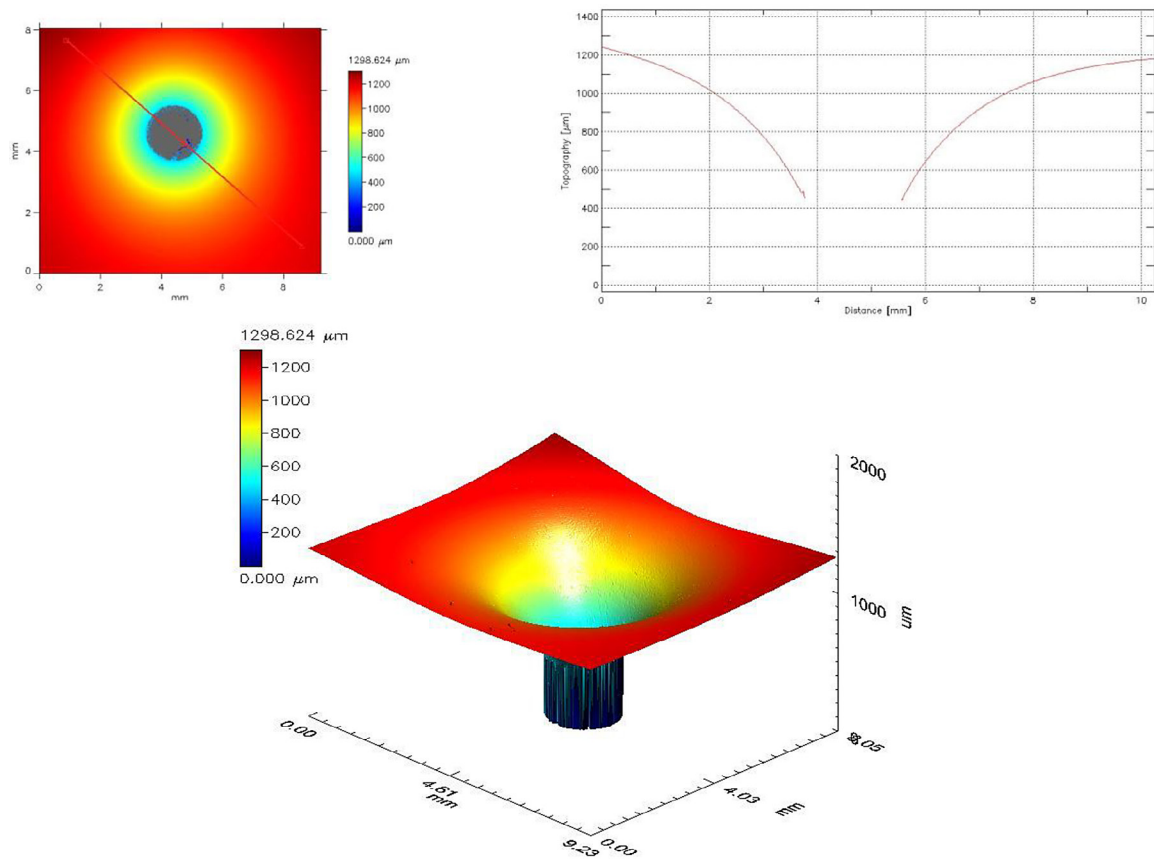


Figure 11. Visualization of the hole formed by the profilometer on VST tested for specimen by 23 °C temperature conditioning

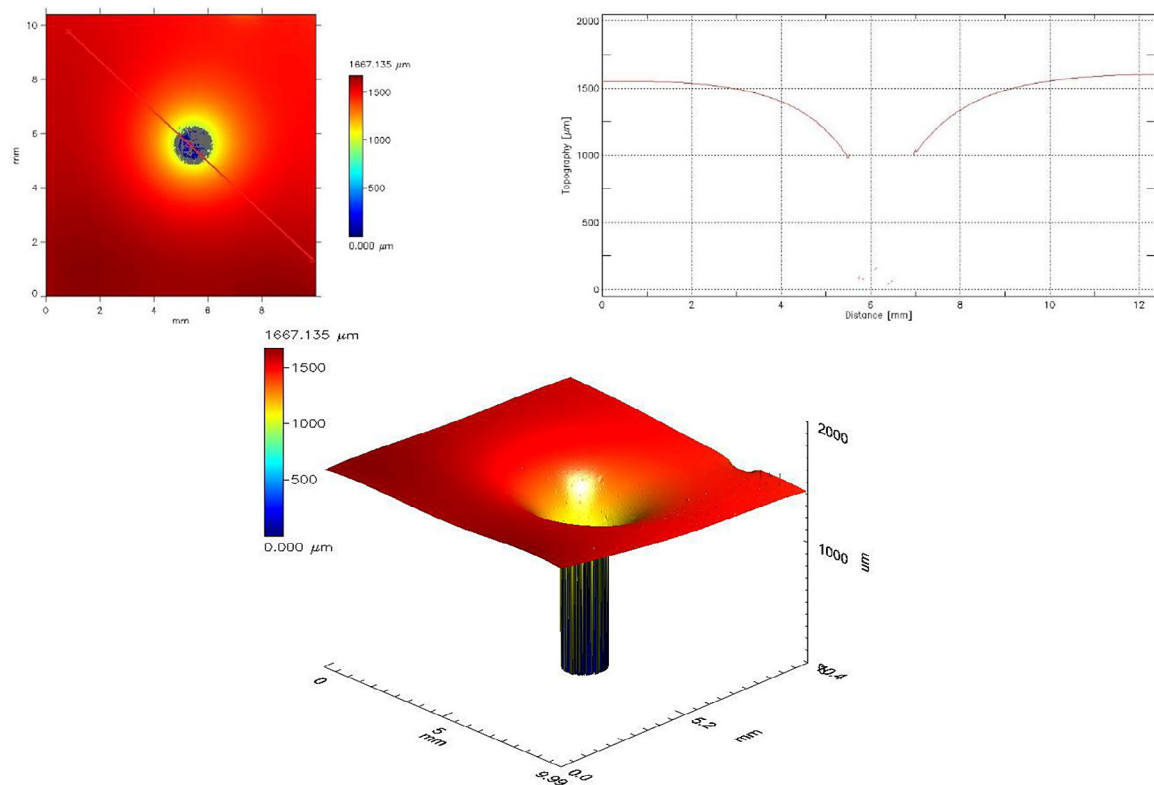


Figure 12. Visualization of the hole formed by the profilometer on VST tested for specimen by 55 °C temperature conditioning

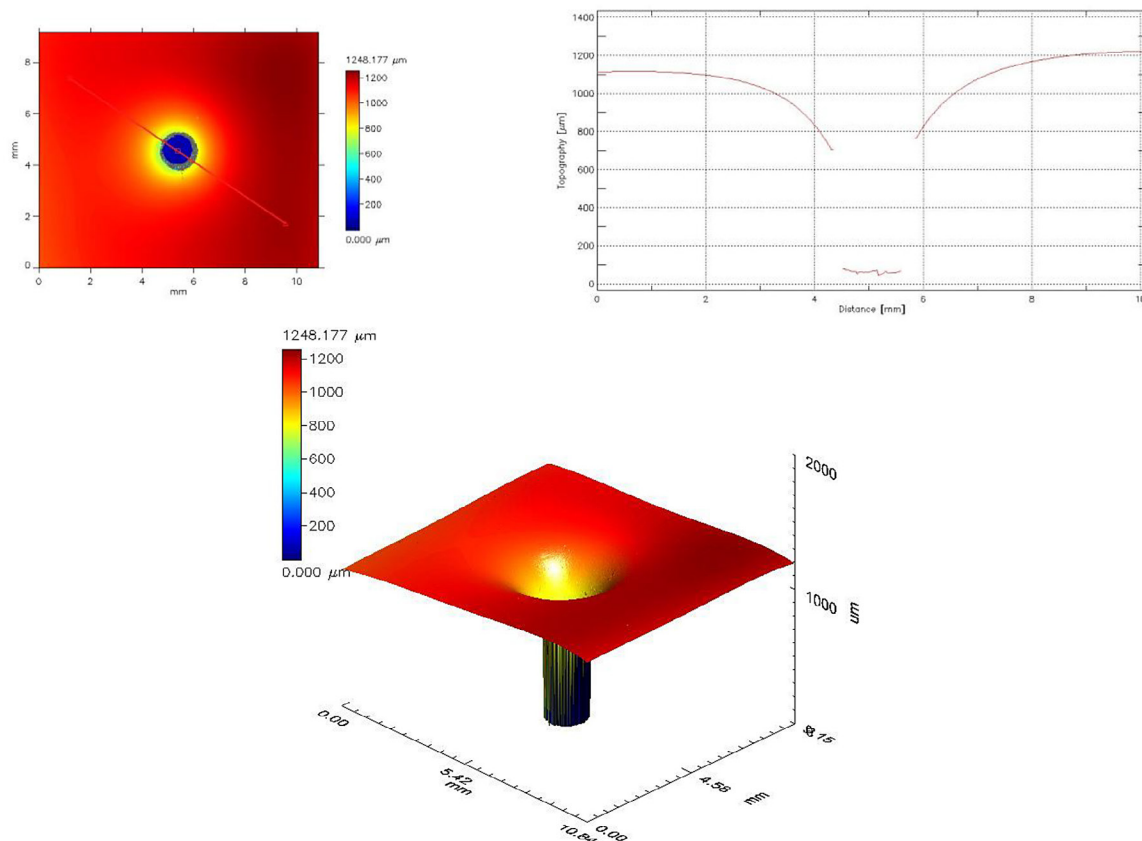


Figure 13. Visualization of the hole formed by the profilometer on VST tested for specimen by 80 °C temperature conditioning

the bottom of the hole, resulting in a flat surface resembling the indenter tip.

DISCUSSION

The values of the arithmetic mean, and median do not differ significantly from each other. Also, the values of the standard deviation of the mean are not large, which means that the data obtained do not show a large scatter of test results. This is also evident in Figures 14 and 15.

The results show that there is a noticeable increase in the temperature strength of the resin as the annealing temperature increases during sample fabrication. The nature of the increase is close to linear (high correlation coefficient) and independent of the measurement temperature or load. Nevertheless, as expected, a slight decrease in the temperature strength of the specimens is observed as the load increases during measurement. On the other hand, the marked increase in use temperature during measurement with a larger temperature increase over time during heating

allows the assumption that additional hardening of the material on the sample surface occurs to a much greater extent than at a lower heating rate.

During the tests, not all specimens reached the required 1 mm recess value. This is associated with the low force value set during the test. Of the four methods used, the method with a 10 N force did not result in the specimens reaching the required displacement. However, an anomaly was observed with the RT14 sample. This specimen did reach the required displacement for the 10 N force method, which may be due to the presence of an air bubble inside the specimen. As a result, it was decided that for these samples, the “virtual” softening temperature would be determined. This involves calculating the temperature at the intersection of two tangent lines drawn to the experimental curve as a function of temperature. The first line is tangent to the linear increase in depression, and the second is tangent to the stabilized depression value. The “virtual” softening temperature is marked in red in the tables. The determined temperature of the arbitrary softening of the material is presented in red in the summary

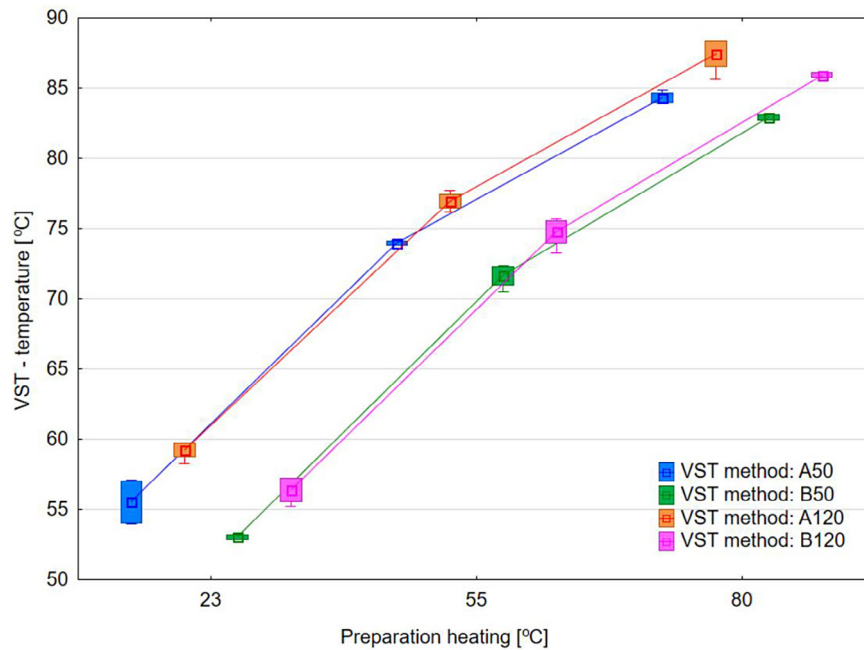


Figure 14. VST results in the form of graphs with extreme values and standard deviation of the mean indicated

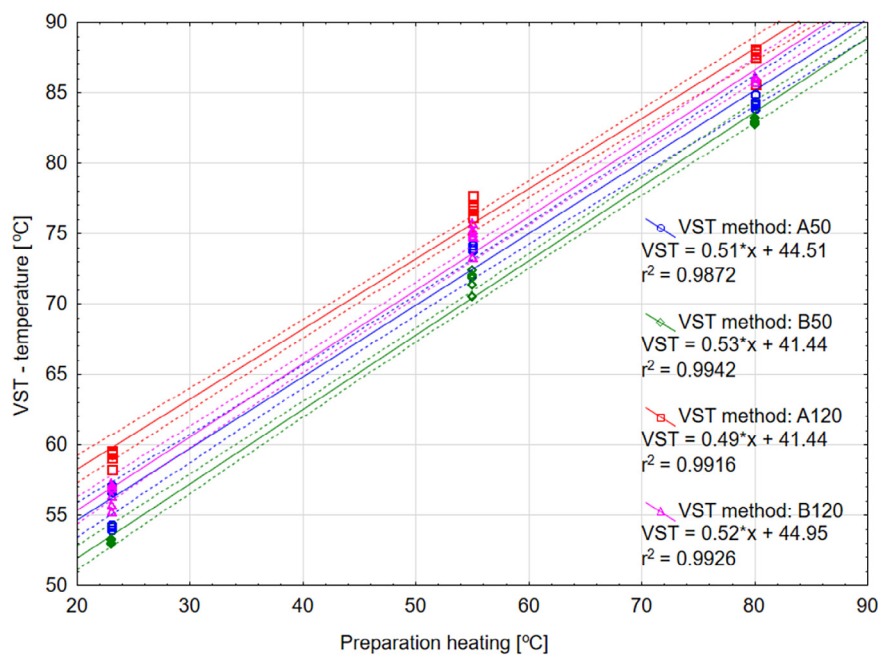


Figure 15. VST results: scatter plots with marked 0.95 confidence interval and linear approximation functions

tables. Based on the results obtained, it can be concluded that the conditioning temperature did influence the achieved softening point. The samples conditioned at room temperature showed the lowest VST values, while the highest softening point was characteristic for samples conditioned at 80 °C across all methods used. When considering the heating rate, it did not have a significant impact on the results.

The samples subjected to the HDT test reached different deflection temperatures under load, depending on the conditioning temperature and the method used. Specimens conditioned at room temperature exhibited the lowest heat deflection temperature under load, while those conditioned at 80 °C showed the highest values. The method used also influenced the shape of the resulting chart. Specimens tested according

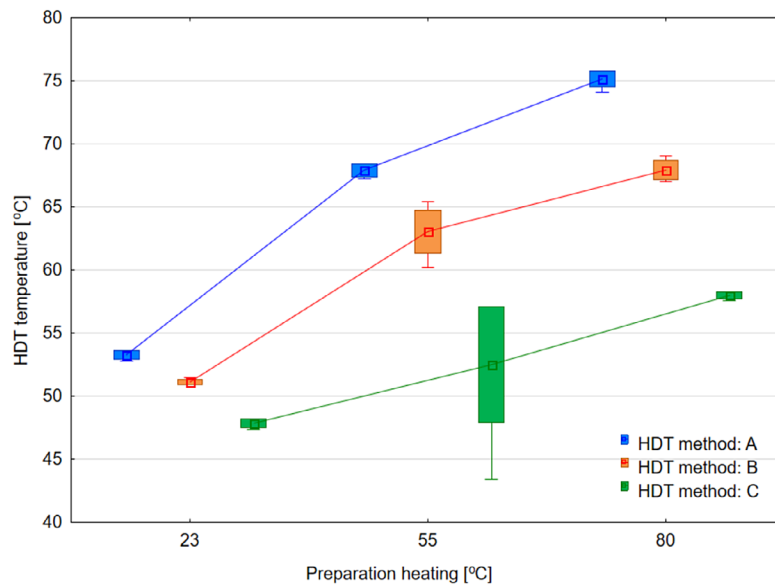


Figure 16. HDT results in the form of graphs with extreme values and standard deviation of the mean indicated

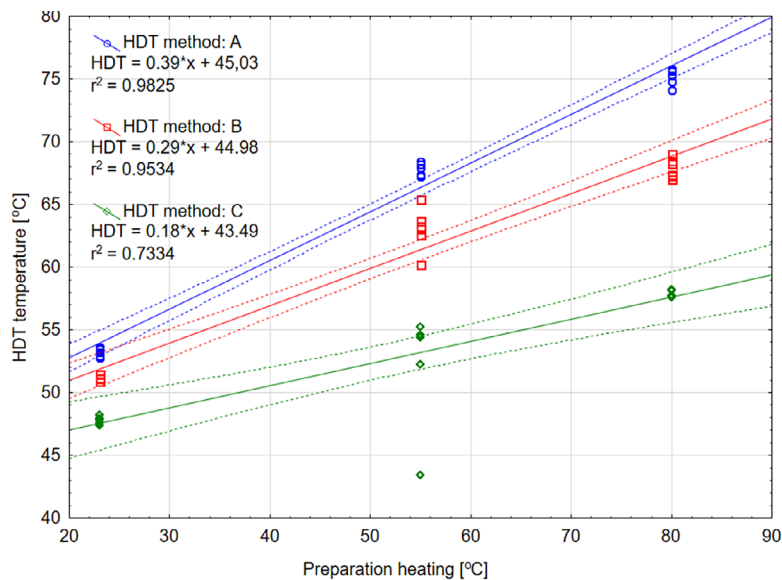


Figure 17. HDT results: scatter plots with marked 0.95 confidence interval and linear approximation functions

to method B parameters (i.e., bending stress of 0.45 MPa) displayed a relatively flat curve in the initial phase, followed by a sudden increase in the final phase. In contrast, the characteristics of the samples tested with method C, due to the higher applied pressure force, showed a more gradual increase in displacement at lower heating temperatures.

One of the diagrams for the C120 method, for specimen number 5517 conditioned at 55 °C, displayed a different characteristic compared to the others. This anomaly may be linked to a defect in the sample, specifically air entering the resin.

This resulted in a larger standard deviation (Table 5), as well as a poorer fit of the approximating function to the measurement results, as indicated by a worse r^2 value (Figure 16 and 17).

CONCLUSIONS

Conclusions from the study:

- The conditioning temperature of the epoxy resin samples has a significant impact on the measured VST and HDT. Thermal pre-treatment alters the molecular arrangement within

the polymer matrix, affecting its thermal resistance [31–33].

- The VST B50 method, utilizing a 50 N load and a low heating rate of 50 °C/h, produced the lowest thermal resistance values among all test configurations. These parameters reflect conservative service conditions, making this method useful for evaluating the upper operating temperature limits of the material.
- The heating rate in the Vicat test did not significantly influence the softening temperature, indicating limited kinetic sensitivity of the tested epoxy resin under the applied conditions.
- Dimensional consistency of the specimens was effectively achieved through the free casting method in silicone molds, which enabled high repeatability in thermomechanical tests.
- The transparent nature of the epoxy resin hampered effective surface mapping using optical profilometry. The use of surface dyes or coatings is recommended for future surface characterization workflows [34].
- Investigation into the long-term thermal aging behavior of epoxy resin to assess mechanical and thermal stability over extended service periods [35].
- Evaluation of the effect of various reinforcement materials (e.g., glass or carbon fibers) on the composite's VST, HDT, and structural integrity.
- Study of the influence of environmental factors (e.g., humidity, UV radiation, thermal cycling) on the thermal and mechanical degradation of the resin system.
- Future research may focus on the long-term thermal aging of the resin, the impact of different reinforcement materials, and the influence of environmental factors on its thermal and mechanical properties.

REFERENCES

1. Elhousari, A. M., Rashad, M., Elsheikh, A. H., and Dewidar, M. The effect of rubber powder additives on mechanical properties of polypropylene glass-fiber-reinforced composite, *Mech. Sci.*, 2021;12:461–469, <https://doi.org/10.5194/ms-12-461-2021>
2. Borowiec M., Gawryluk J., Bochenski M. Influence of mechanical couplings on the dynamical behavior and energy harvesting of a composite structure. *Polymers* 2021;13:66. <https://doi.org/10.3390/polym13010066>
3. Sławski S., Szymiczek M., Kaczmarczyk J., Domin J., Świtoński E. Low velocity impact response and tensile strength of epoxy composites with different reinforcing materials. *Materials* 2020;13:3059. <https://doi.org/10.3390/ma13143059>
4. Kosicka E, Borowiec M, Kowalczyk M, Krzyzak A, Szczepaniak R. influence of the selected physical modifier on the dynamical behavior of the polymer composites used in the aviation industry. *Materials* 2020;13:5479. <https://doi.org/10.3390/ma13235479>
5. Komorek A., Szczepaniak R., Przybyłek P., Komorek K., Komorek Z., Godzimirski J., Zbrowski A. Temperature Rise of an Adhesive Particle-Reinforced Polymer during Fatigue Testing. *Polymers* 2023;15:742. <https://doi.org/10.3390/polym15030742>
6. Szczepaniak R., Kozun G., Przybyłek P., Komorek A., Krzyzak A., Woroniak G. The effect of the application of a powder additive of a phase change material on the ablative properties of a hybrid composite. *Composite Structures* 2021; 256: 113041. <https://doi.org/10.1016/j.compstruct.2020.113041>
7. Ramesh M., Arun Ramnath R., Deepa C. Chapter 12 – Friction and wear properties of carbon nanotube-reinforced polymer composites, Elsevier, 2021, Pages 223-240, <https://doi.org/10.1016/B978-0-12-819767-7.00012-8>
8. Mrówka M., Woźniak A., Prężyna S., Sławski S. The influence of Zinc waste filler on the tribological and mechanical properties of silicone-based composites. *Polymers* 2021;13:585. <https://doi.org/10.3390/polym13040585>
9. Yogeshwarana S., Natrayan L., Rajaraman S., Parthasarathi S., Nestro S. Experimental investigation on mechanical properties of epoxy/graphene/fish scale and fermented spinach hybrid bio composite by hand lay-up technique. *Materials Today: Proceedings* 2021;37(2):1578–1583. <https://doi.org/10.1016/j.matpr.2020.07.160>
10. McIlhagger A., E. Archer E., McIlhagger R. Manufacturing processes for composite materials and components for aerospace applications, *Polymer Composites in the Aerospace Industry* (Second Edition), 2020:59–81, <https://doi.org/10.1016/B978-0-08-102679-3.00003-4>
11. Liu Y., Guan Y., Hu G., Zhai J., Chen F., Lin J. Study on properties of BF/PP composites and plastic parts manufacturing by mold opening foaming injection molding, *Composite Structures*, 2023;321:117295, <https://doi.org/10.1016/j.compstruct.2023.117295>
12. Gooch J. W. Heat Deflection Temperature. In: Gooch J.W. (eds) *Encyclopedic Dictionary of Polymers*. Springer. 2011 (New York, USA). https://doi.org/10.1007/978-1-4419-6247-8_5831
13. Gooch J. W. Vicat test. In: Gooch J.W. (eds) *Encyclopedic Dictionary of Polymers*. Springer. 2011 (New York, USA). https://doi.org/10.1007/978-1-4419-6247-8_12522

14. Toldy A., Szolnoki B., Marosi Gy. Flame retardancy of fibre-reinforced epoxy resin composites for aerospace applications, Budapest, 2011.
15. Gannon J. A. History and development of epoxy resins., 1986.
16. Botezatu C., Oroian B., Hrituc A., Condrea I. Influences of the circular economy in industrial engineering. IOP Conference Series, 2019.
17. Epoxy Resins Market Analysis by Mordor Intelligence: <https://www.mordorintelligence.com/industry-reports/global-epoxy-resin-market-industry>, 2025.
18. Xuesong Z. Recent advances in the development of aerospace materials. Progress in Aerospace Science., 2018:22–34. <https://www.semanticscholar.org/>
19. <https://www.pinterest.cl/> [Online]
20. Barile C., Casavola C., De Cillis F. Mechanical comparison of new composite materials for aerospace applications. Composites Part B: Engineering, 2019;162:122–128.
21. Holmes M. Aerospace looks to composites for solutions. Reinforced Plastics, 2017;61:237–241.
22. Ma J., Shen L., He Y. Application of composite materials in engine. Advanced Composite Materials, 2017.
23. China Aviation Daily. 12 04 2014. <http://www.chinaaviationdaily.com/news/34/34237.html>
24. Johnson A. F. Design and testing of crashworthy aerospace composite components. Polymer Composites in the Aerospace Industry, 2015:261–293.
25. Alemour B., Omar Badran O., Hassan M. R. A review of using conductive composite materials in solving lightning strike and ice accumulation problems in aviation, J Aerosp Technol Manag 2019;11.
26. Głogowska K., Majewski Ł., Garbacz T., Tor-Świątek A. The effect of ageing on selected properties of polylactide modified with blowing agents. Advances in Science and Technology Research Journal, 2019;13(4):204–213. <https://doi.org/10.12913/22998624/112025>
27. ISO 306 Plastics – Determination of Vicat softening temperature (VST), United Test, 2017.
28. ISO 75-2:2013 Plastics – Determination of temperature of deflection under load – Part 2: Plastics and ebonite, United Test, 2013.
29. Havel-composites. Havel Composites PL Sp. z o.o. <http://www.havel-composites.pl>
30. Gu J., Bai Y., Zhao Z., Zhang C. Temperature and strain rate sensitivity of modulus and yield strength of epoxy resin under compressive loads. Polymer, 2024;295. <https://doi.org/10.1016/j.polymer.2024.126744>
31. Mucha M., Sterzyński T., Krzyżak A. The effect of the heat treatment on the crosslinking of epoxy resin for aviation applications. Polimery, 2020, <https://dx.doi.org/10.14314/polimery.2020.11.4>
32. Luiza de Lemos A., Galera Prestes Pires P., Lopes de Albuquerque M, Vagner Roberto Botaro V., Faulstich de Paiva J. M. Biocomposites reinforced with natural fibers: thermal, morphological and mechanical characterization. BCCM3 - Brazilian Conference on Composite Materials, 2017; artigo e-11840, <https://doi.org/10.1590/s1517-707620170002.0173>
33. Gupta R., Mallikarjuna D., Baines L., Flynn D., Bucknall D. Quantification of wear in glass reinforced epoxy resin composites using surface profilometry and assessing effect of surfacing film involvement. Materials Today: Proceedings, 2022;57(Part 2):930–935. <https://doi.org/10.1016/j.matpr.2022.03.061>
34. Benedetti A., Fernandes P., Granja J. L., Sena-Cruz J., Azenha M. Influence of temperature on the curing of an epoxy adhesive and its influence on bond behaviour of NSM-CFRP systems, Composites Part B, 2015, <https://doi.org/10.1016/j.compositesb.2015.11.034>